ELECTROWEAK RESULTS FROM NUTEV

Robert B. Drucker

University of Oregon

Eugene, OR 97403

Representing the NuTeV Collaboration

ABSTRACT

We report our measurement of the weak mixing angle, $\sin^2 \theta_W$, in neutrino–nucleon deep inelastic scattering in the NuTeV experiment at Fermilab. Using separate neutrino and antineutrino beams, we are able to use the Paschos-Wolfenstein relations to extract $\sin^2 \theta_W$ with low systematic errors. Our preliminary result is $\sin^2 \theta_W^{(on-shell)} \equiv 1 - m_W^2/m_Z^2 = 0.2253 \pm 0.0019(stat.) \pm 0.0010(syst.)$, which in the Standard Model is equivalent to a W mass measurement of $80.26 \pm 0.11 \text{ GeV}/c^2$.

1 Introduction

Neutrino scattering experiments have played an important role in the development of the electroweak standard model. Precision measurements of neutrino-nucleon (νN) neutral current (NC) to charged current (CC) ratios contributed to predictions of the W, Z, and top quark masses before these particles were directly observed. Today, in conjunction with the large samples of direct Z and W production from collider experiments, precision measurements from νN scattering can help constrain the mass of the Higgs boson. Neutrino-nucleon scattering results are also sensitive to a variety of non-Standard Model physics, including extra Z bosons, leptoquarks, quark compositeness, and neutrino oscillations.[1-3]

In the past, neutrino experiments have had a large common systematic uncertainty due to charm quark production.[4-6] Production of charm quarks from low-x sea quarks has large systematic uncertainties associated with the effective mass suppression, see Fig. 1. The NuTeV experiment ran in separate neutrino and antineutrino modes, which greatly reduces the sea quark uncertainties by using the quantity suggested by Paschos and Wolfenstein[7] for measuring the weak mixing angle:

$$R^- \equiv \frac{\sigma_{NC}^{\nu N} - \sigma_{NC}^{\bar{\nu} N}}{\sigma_{CC}^{\nu N} - \sigma_{CC}^{\bar{\nu} N}} = \frac{1}{1-r}\left(\frac{\sigma_{NC}^{\nu N}}{\sigma_{CC}^{\nu N}} - r\frac{\sigma_{NC}^{\bar{\nu} N}}{\sigma_{CC}^{\bar{\nu} N}}\right) \equiv \frac{R^\nu - rR^{\bar{\nu}}}{1-r}, \tag{1}$$

where $r \equiv \sigma_{CC}^{\bar{\nu} N}/\sigma_{CC}^{\nu N} \approx 1/2$. Since R^- is a function of the difference between neutrino and antineutrino cross sections, effects from sea quarks tend to cancel.
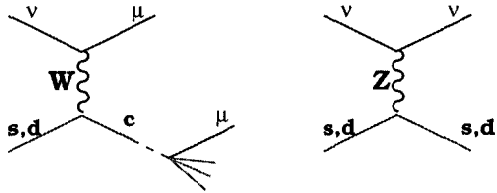

Figure 1: Feynman diagrams showing how a charm quark is produced in νN scattering. Note that this process only occurs in the charged current events; therefore, it alters the NC/CC ratio.

The $\sin^2\theta_W$ measured in νN scattering is approximately the on-shell mixing angle, $\sin^2\theta_W^{on-shell} \equiv 1 - m_W^2/m_Z^2$. Our result, therefore, can be compared with direct measurements of the mass of the W boson by collider experiments. This comparison is relatively insensitive to uncertainties in the top quark mass. A

discrepancy between the NuTeV measurement of the W mass and other direct measurements would arise in the various Standard Model extensions mentioned above.

2 The NuTeV Experiment

The NuTeV detector consists of a 690 ton iron-scintillator calorimeter, followed by an iron toroidal spectrometer, see Fig. 2. The calorimeter consists of 168 steel plates, each 3 m × 3 m × 5.15 cm, instrumented with liquid scintillator counters placed after every two steel plates and drift chambers after every four plates. The calorimeter has a total length of 18 m and an average density of 4.2 g/cm^3. The muon spectrometer consists of three toroidal magnets with magnetic fields varying from 1.7 T near the center to 1.5 T near the edge. Drift chambers are positioned downstream of each of the toroids for tracking the muon trajectory and determining the muon momentum. The toroid spectrometer is not used directly in this analysis, but it is used to measure the neutrino flux from the beamline.
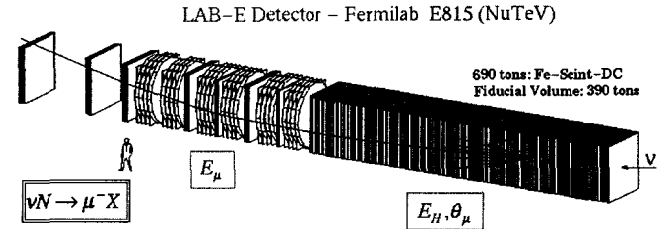

Figure 2: A drawing of the NuTeV detector, showing the calorimeter and the toroidal spectrometer. The figure includes a drawing of a charged current event showing the incoming neutrino, the hadronic shower in the calorimeter, and the muon going through the spectrometer.

The NuTeV beamline, known as the Sign Selected Quadrupole Triplet (SSQT), received 3×10^{18} protons at 800 GeV from the Fermilab Tevatron during the 1996-97 fixed-target run. Figure 3 shows a diagram of the SSQT elements. Pions and kaons of one charge are bent by a dipole immediately downstream of the BeO target. Neutral and wrong-sign particles were stopped in beam dumps. A quadrupole magnet triplet then focuses the beam into the 0.5 km decay region. The center of the decay region is 1.3 km from the NuTeV detector. Figure 4 shows

the predicted flux for the NuTeV neutrino beam. Measured $\bar{\nu}_\mu$ contamination in the ν_μ beam is less than 1/1000, and ν_μ contamination in the $\bar{\nu}_\mu$ beam is less than 1/500. Electron neutrinos in the beam account for 1.3% of the observed interactions in neutrino mode and 1.1% in antineutrino mode.
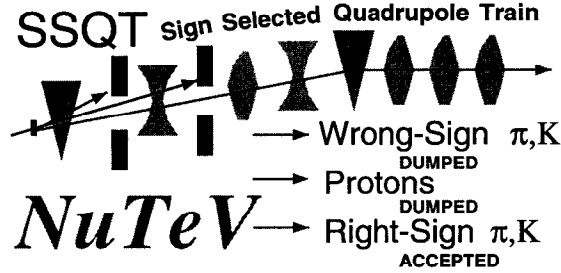

Figure 3: This diagram shows the elements of the NuTeV beamline SSQT elements. The protons enter from the left and hit the BeO target shown as a small rectangle in the picture. The wrong-sign and neutral secondaries are dumped in the beam dumps, and the right-sign particles are focused into the decay space.

Event length in the detector, defined as the number of scintillation counters with signal in them, is used to separate NC and CC events. Figure 5 shows examples of NC and CC candidate events in the NuTeV detector. CC events appear long in the detector because they contain a muon in the final state. NC events only have a short range hadronic shower. Experimentally, the ratio of NC to CC events is measured by the ratio of the number of short to long events.

Contamination in the beam from ν_e interactions alters the ratio of short to long events, because CC ν_e events do not contain a final state muon and so appear short. Figure 6 shows the length distributions separately for CC, NC, and electron neutrino events. It is critical to have a precise understanding of the number of electron neutrino events in the beam. Most of the ν_e contamination comes from $K_{e3}^\pm$ decay (93% in the ν_μ beam and 70% in the $\bar{\nu}_\mu$ beam). We use a Monte Carlo to estimate the number of electron neutrinos from $K_{e3}^\pm$ decay. The Monte Carlo was tuned to agree with the number of observed $\nu_\mu/\bar{\nu}_\mu$ events. Figure 7 shows the ν_μ energy distribution and a comparison with the Monte Carlo. The SSQT was very precisely aligned, which leads to a very well understood prediction of the number of $K_{e3}^\pm$ decays. The estimate for the number of $\nu_e/\bar{\nu}_e$ from $K_{e3}^\pm$ decays is accurate to approximately 1.5%, and is dominated by the
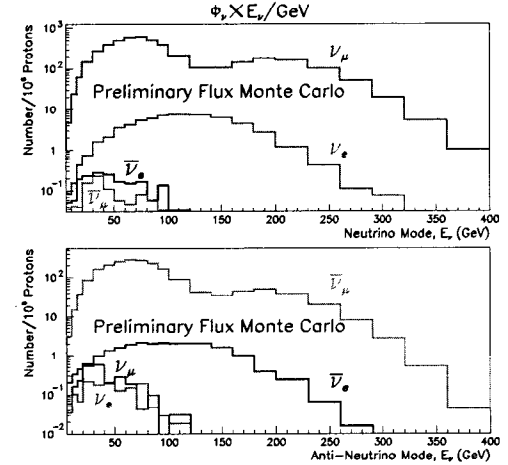

Figure 4: This plot shows the predicted number of νN events from the NuTeV beam as a function of neutrino energy. The upper plot is for neutrino mode and the lower plot is anti-neutrino mode. Note the very small contamination of "wrong-sign" neutrinos.

uncertainty in the measured $K_{e3}^\pm$ branching ratio. Uncertainties on neutral kaon production and decay are much larger, but the SSQT design greatly reduces the acceptance for neutrinos from neutral particle decays.

NuTeV had a separate calibration beamline that delivered beam during each 60 second accelerator cycle. Calibration data with muons, pions, and electrons were recorded throughout the entire run. This provided a large sample of calibration data as well as a constant monitor of detector performance and calibration.

3   Event Selection

Events used for this analysis are required to deposit at least 20 GeV in the calorimeter to ensure efficient triggering and good vertex reconstruction. The event vertex is required to be in the fiducial region of the detector. In the transverse dimensions, we require the vertex to be in the central two-thirds of the calorimeter, in order to reduce losses of final state particles out the sides of the detector. The longitudinal position of the vertex is required to be at least 0.4 m
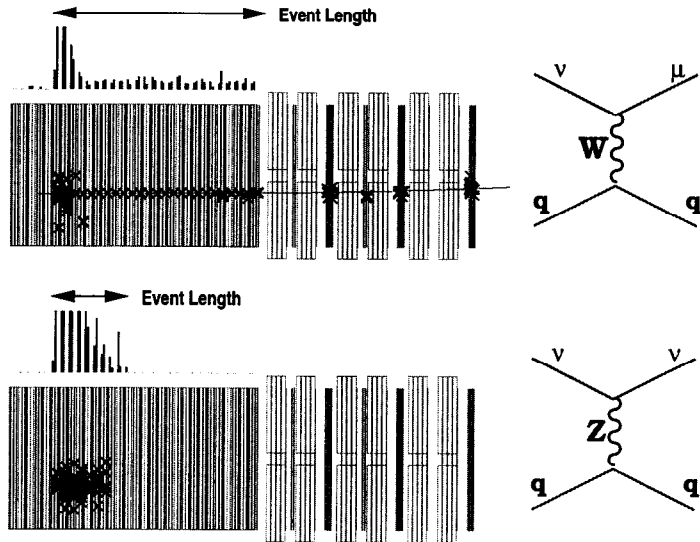
Figure 5: Event displays of a NuTeV charged current candidate and a neutral current candidate. The X's are hits in the tracking chambers and the vertical bars above the calorimeter show the energy recorded in each scintillation counter. This figure illustrates the definition of "long" and "short" events.

steel-equivalent from the upstream end of the calorimeter to ensure that the event was neutrino induced, and at least 2.4 m steel-equivalent from the downstream end to ensure that a minimal event length can be measured. Cosmic-ray events are a small background, and they are statistically subtracted using events taken during beam-off gates. Muon-induced events are also statistically subtracted using events recorded while the beam was on. After all cuts, 1.3 million neutrino and 0.3 million antineutrino events are observed.

4   Extraction of $\sin^2 \theta_W$

Figure 8 shows the measured event length distributions for the neutrino and anti-neutrino samples. Long events, considered CC candidates, are those that penetrate more than 20 counters, or 2 m steel-equivalent. The ratio of short to long events in neutrino mode is $R^\nu_{meas.} = 0.4198 \pm 0.0008$, and in antineutrino mode $R^{\bar\nu}_{meas.} = 0.4215 \pm 0.0017$.
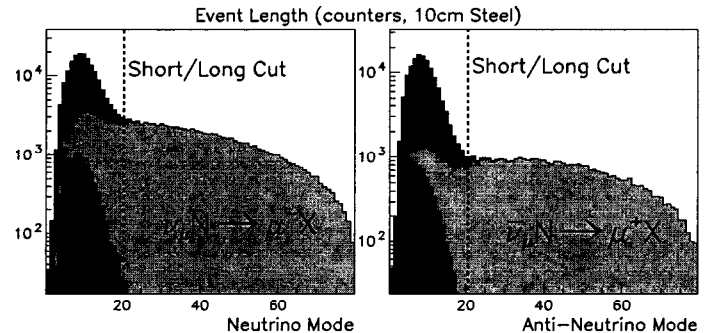

Figure 6: This figure shows the number of neutrino events as a function of event length. The separate contributions from charged current, neutral current, and electron neutrino events are shown. Note that the ν_e events only contribute to the short event sample.

$\sin^2 \theta_W$ is extracted using a detailed detector Monte Carlo simulation. The Monte Carlo must carefully simulate all detector and cross-section effects that cause cross-talk between the long and short event samples.

Several detector effects must be considered to properly simulate the expected event length distribution. For CC events the event length is affected by the scintillation counter efficiency, noise, and active area. These properties were measured using neutrino data and muons from the calibration beam. Determining the event vertex position is critical to the length measurement. Vertex finding resolutions and biases were studied using a detailed GEANT simulation of the detector. Vertex position bias was also checked using the CCFR two-muon data sample, which allows a very precise independent vertex position measurement from the two muon tracks. It is also important to carefully model the length distribution of hadronic showers, since they determine the event length in the NC sample. The hadronic shower length was studied using calibration beam pions. As a check, shower lengths from a sample of calibration beam kaons were also studied, because neutrino-induced events contain a mixture of pion and kaon secondaries. No significant differences were observed between the pion and kaon shower lengths. Figure 9 shows the hadronic shower lengths from the calibration beam pions compared with the tuned Monte Carlo simulation. The Monte Carlo does an excellent job of reproducing the hadronic shower length.

The Monte Carlo used a leading-order cross-section model for neutrino-nucleon
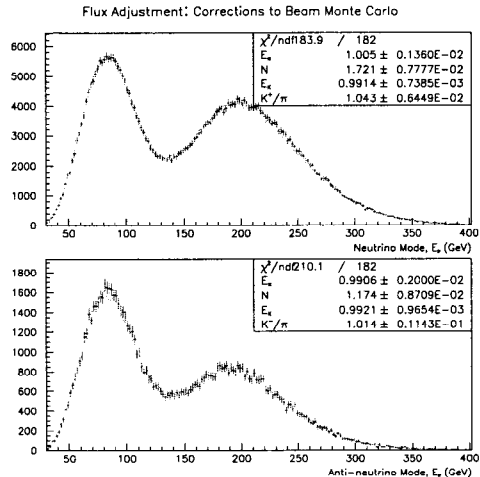
Figure 7: The NuTeV neutrino flux measured using a sample of charged current events. The plots show the number of neutrino events as a function of neutrino energy; the upper plot is neutrino mode and the lower plot is antineutrino mode. The peak near 90 GeV is due to pion decay and the peak near 200 GeV is from kaon decay. The solid lines show the Monte Carlo flux used in the analysis. The Monte Carlo was tuned slightly (within errors) to match the data.
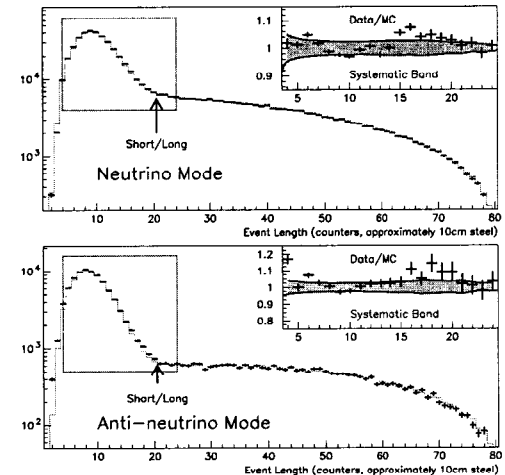

Figure 8: These plots show the number of events as a function of the event length. The solid curve is Monte Carlo, and shows excellent agreement with the data.

deep inelastic scattering, and also included neutrino-electron and quasi-elastic scattering. Leading-order parton distribution functions, as measured by the CCFR experiment[8] and fit with the Buras-Gaemers parameterization,[9] were used. CCFR was the predecessor to NuTeV and used the same calorimeter as NuTeV. These parton distribution functions were modified to include measured u/d valence asymmetries and sea quark asymmetries.[10,11] The strange sea distribution used was that measured by CCFR from its two-muon sample.[12] Mass suppression effects for heavy quark production are modeled using slow rescaling, with parameters taken from the CCFR two-muon data.

Electroweak and QED radiative corrections to the scattering cross sections are applied using a computer program supplied by Bardin.[13] The charm sea was included using CTEQ4L parton distribution functions,[14] and was assigned a 100% systematic. The longitudinal structure function, R_L, used was based on QCD predictions and data.[15] Higher-twist effects[16] (effects from the nuclear environment of the interaction) were included with a 100% systematic.

$\sin^2 \theta_W$ was extracted from the data by varying the value of $\sin^2 \theta_W$ used in the Monte Carlo until the predicted NC/CC ratios agreed with the data. The comparison with data was based on the quantity

$$\hat{R}^-_{meas.} \equiv R^\nu_{meas.} - \alpha R^{\bar\nu}_{meas.},$$

where $\alpha = 0.5136$ was chosen, using the Monte Carlo, to minimize the systematic uncertainty due to charm quark production. Note that $\hat{R}^-_{meas.}$ is quite close to being R^- as defined in Eq. (1). Using $\hat{R}^-_{meas.}$, which is possible because of NuTeV's ability to run separate neutrino and antineutrino beams, greatly reduces many systematic uncertainties from sea quark effects and other correlated systematics. Figure 10 shows the $R^\nu_{meas.}$ and $R^{\bar\nu}_{meas.}$ distributions as a function of energy deposited in the calorimeter. Figure 11 shows the $\hat{R}^-$ distribution. The Monte Carlo agrees well with the data. Note that there appear to be slight systematic wiggles in the $R^\nu_{meas.}$ and $R^{\bar\nu}_{meas.}$ distributions, but they are correlated and cancel out in the $\hat{R}^-_{meas.}$ plot. This is exactly the reason for using $\hat{R}^-$.
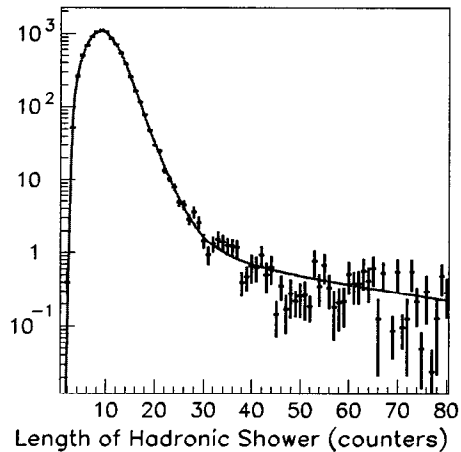
Figure 9: Length of hadronic showers in the NuTeV calorimeter. The points show the number of events as a function of event length for calibration beam pions. The solid curve is the Monte Carlo modeling of the event length. The agreement is excellent.

Table 1 shows a summary of the systematic uncertainties in the $\sin^2\theta_W$ measurement. The total error is dominated by statistical uncertainty. Note how small the charm mass effect error is with this R^- analysis.

5 Results

The preliminary result for $\sin^2\theta_W$ from NuTeV is

$$
\begin{aligned}
\sin^2\theta_W{}^{(on-shell)} &= 0.2253 \pm 0.0019(stat.) \pm 0.0010(syst.) \\
&\quad -0.00142 \times \left(\frac{M_{top}{}^2 - (175 \text{ GeV})^2}{(100 \text{ GeV})^2} \right) \\
&\quad +0.00048 \times \log_e \left(\frac{M_{Higgs}}{150 \text{ GeV}} \right).
\end{aligned} \tag{2}
$$

This result represents a factor of three improvement in systematic uncertainty over the previous best νN result. The small residual dependence of our result on M_{top} and M_{Higgs} comes from the leading terms in the electroweak radiative corrections.[13] Figure 12 shows the NuTeV result in the M_W–M_{top} plane. Since

Table 1: This table shows a summary of all the NuTeV systematic uncertainties. Note that the uncertainty in the measurement is dominated by the statistical error. Note also the very small uncertainty associated with the charm mass.

| Source of Uncertainty		$\delta\sin^2\theta_W$
Statistics:	Data	0.00188
	Monte Carlo	0.00028
Total statistics		**0.00190**
$\nu_e/\bar\nu_e$ *Flux:*	$K^\pm$ (1.1%)	0.00024
	Other sources of ν_e's	0.00048
Energy measurement: Calibrations (0.5%)		0.00043
	Muon energy deposition (3%)	0.00004
	Energy resolution	0.00004
Event length:	Hadron shower	0.00015
Longitudinal vertex determination		0.00015
	Counter edge location	0.00010
	Counter efficiency and noise	0.00016
Total experimental systematics		**0.00075**
Sea quarks:	Strange Sea	0.00034
	V_{cd}	0.00004
	Charm sea	0.00009
	Charm mass	0.00009
Other $\nu/\bar\nu$ cross-section differences: $\sigma^\nu/\sigma^{\bar\nu}$		0.00023
	Nonisoscalar target	0.00013
	Radiative corrections	0.00051
Non-QPM cross section:	Higher twist	0.00013
	Longitudinal structure function	0.00007
Total physics model		**0.00070**
Total uncertainty		**0.0022**
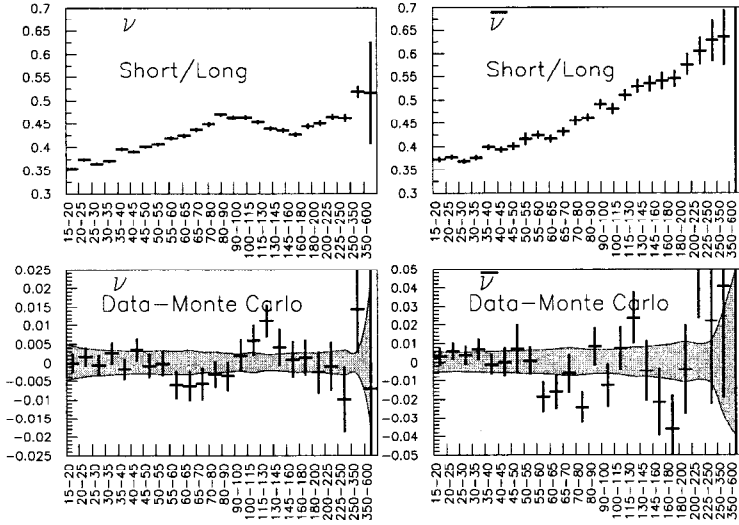
Figure 10: The upper plots show the $R^\nu_{meas.}$ and $R^{\bar\nu}_{meas.}$ distributions from the NuTeV data as a function of hadronic shower energy. The lower plots show the difference between the data and the Monte Carlo predictions. The band shows the systematic uncertainty. The Monte Carlo is in good agreement with the data. There are slight correlated wiggles in the data, within the errors. The advantage of using R^- is that these correlated effects subtract out.

$\sin^2\theta_W{}^{\text{(on-shell)}} \equiv 1 - M_W^2/M_Z^2$, this result is equivalent to

$$
\begin{aligned}
M_W =\ & 80.26 \pm 0.10(stat.) \pm 0.05(syst.) \\
& +0.073 \times \left(\frac{M_{top}{}^2 - (175 \text{ GeV})^2}{(100 \text{ GeV})^2} \right) \\
& -0.025 \times \log_e \left(\frac{M_{Higgs}}{150 \text{ GeV}} \right).
\end{aligned} \tag{3}
$$

A comparison of this result with direct measurements of M_W is shown in Fig. 13. The NuTeV result is comparable in precision to the current world direct measurements of the W boson mass.

5.1 Model Independent Couplings

The NuTeV result can be expressed in a more model independent way. The above result has some model dependence in correcting from our measured $\sin^2\theta_W$ to
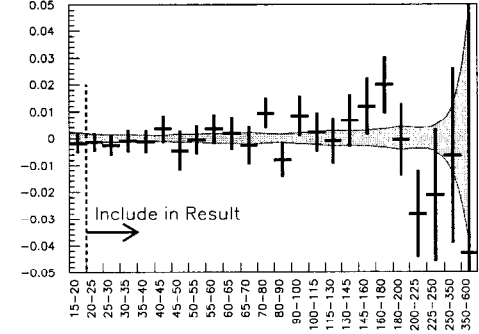

Figure 11: This plot shows the difference between data and Monte Carlo for $\hat{R}^-_{meas.}$ as a function of hadronic shower energy. The band shows the systematic uncertainty. The data and Monte Carlo show excellent agreement. Note that the slight wiggles seen in the $R^\nu_{meas.}$ distributions have no effect on $\hat{R}^-_{meas.}$.

the on-shell value. R^- can be expressed in terms of right- and left-handed quark couplings:

$$
\begin{aligned}
R^- &= \frac{\sigma^\nu_{NC} - \sigma^{\bar\nu}_{NC}}{\sigma^\nu_{CC} - \sigma^{\bar\nu}_{CC}} \\
&= \left(\frac{1}{2} - \sin^2\theta_W \right) \\
&= u_L^2 + d_L^2 - u_R^2 - d_R^2.
\end{aligned}
$$

The variable used in the NuTeV Monte Carlo extraction, $\hat{R}^-_{meas.}$, can be expressed in terms of the quark couplings

$$
\begin{aligned}
0.8587u_L^2 + 0.8828d_L^2 - 1.1657u_R^2 - 1.2288d_R^2 &= 0.2277 \pm 0.0022 \\
&= 0.4530 - \sin^2\theta_W.
\end{aligned}
$$

Figure 14 shows the regions in the g_L^2–g_R^2 plane that the NuTeV measurement allows, where $g_{L,R}^2 \equiv u_{L,R}^2 + d_{L,R}^2$. In order to present the result on the two-dimensional plane, it is assumed that $\delta_{L,R}^2 \equiv u_{L,R}^2 - d_{L,R}^2$ take on the Standard Model values. Also shown in the figure is the region measured by CCFR using R^ν. The CCFR measurement is less precise, but when combined with NuTeV it gives a small allowed region. In the future, the NuTeV data will be used for both
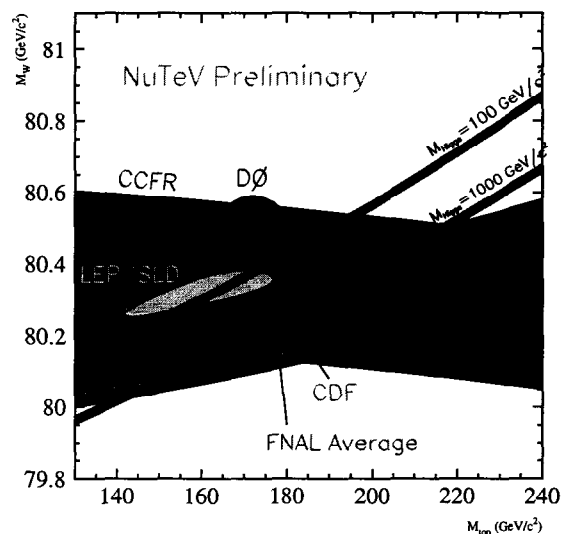
NuTeV Preliminary

CCFR   DØ

LEP SLD

CDF

FNAL Average

M_W (GeV/c²) axis: 81, 80.8, 80.6, 80.4, 80.2, 80, 79.8

M_{top} (GeV/c²) axis: 140 160 180 200 220 240

$M_{Higgs} = 100$ GeV/c² $M_{Higgs} = 1000$ GeV/c²

Figure 12: This plot shows the NuTeV result in the M_W–M_{top} plane compared with other world measurements. The light band is the NuTeV result. The dark band is the CCFR result. The center ellipse shows the combined Fermilab results from NuTeV, CCFR, DØ, and CDF. The Standard Model predictions for $M_{Higgs} =$ 100 GeV/c² and 1000 GeV/c² are shown as narrow bands. The Fermilab and LEP/SLD results tend to slightly favor a light Higgs mass. Note that the NuTeV result depends on the Higgs mass. This dependence is small, and is shown by the side-bands drawn on the NuTeV result which show how much the band would shift in the 100–1000 GeV/c² Higgs mass range.

Value	Experiment
80.36 +/- 0.37	UA2
80.38 +/- 0.12	CDF*
80.43 +/- 0.11	D0
80.35 +/- 0.14	ALEPH*
80.27 +/- 0.16	DELPHI*
80.45 +/- 0.17	L3*
80.36 +/- 0.15	OPAL*
80.375 +/- 0.065	Average
80.26 +/- 0.11	NuTeV*

* : Preliminary

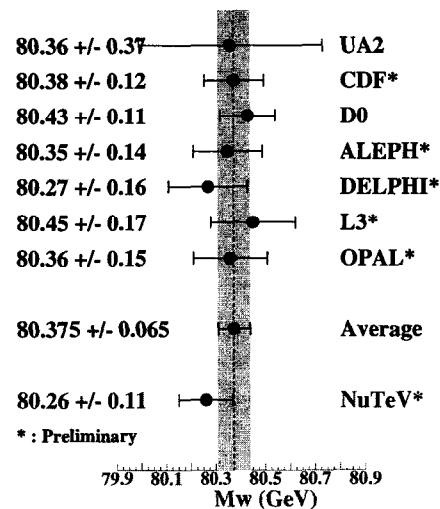79.9   80.1   80.3   80.5   80.7   80.9
Mw (GeV)

Figure 13: The NuTeV result for the W boson mass, compared with other direct measurements. The NuTeV result is currently the most precise direct measurement of the W mass. The NuTeV result is consistent with the other results (unfortunately).

parameters and will reduce the allowed region even further. The plot also shows the Standard Model prediction, which is in good agreement with the data, and therefore, shows no evidence of non-Standard Model physics.

6   Conclusions

NuTeV ran in the Fermilab 1996-1997 fixed-target run and took 3×10^{18} protons on target. By running in separate neutrino and antineutrino modes, we were able to make use of the Paschos-Wolfenstein R^- variable to measure the on-shell weak mixing angle, $\sin^2 \theta_W^{on-shell}$. We have presented a preliminary result that is a factor of two more precise than previous νN scattering experiments. Our result
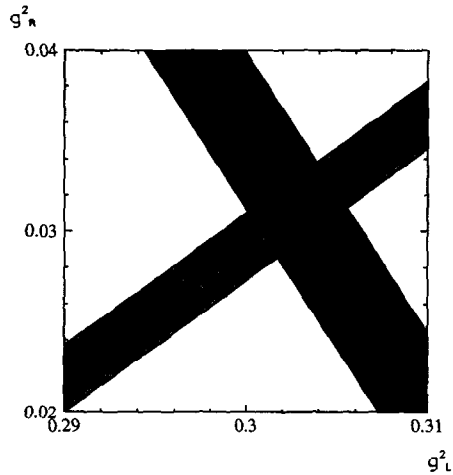
Figure 14: Areas in g_L^2–g_R^2 space allowed by the NuTeV and CCFR model-independent measurements of the quark couplings. Since NuTeV measures R^- and CCFR measures R^ν, the allowed regions for the two experiments are nearly perpendicular. The Standard Model prediction is shown as a point.

is equivalent to a measurement of the W mass and is consistent with other direct measurements of the W mass.

Acknowledgments

References

[1] P. Langacker *et al.*, Rev. Mod. Phys. **64**, 87 (1991).

[2] K.S. McFarland *et al.*, Phys. Rev. Lett **75**, 3993 (1995).

[3] D. Naples *et al.*, Phys. Rev. D **59**, 31101 (1999); E-Print Archive: hep-ex/9809023.

[4] K.S. McFarland, *et al.*, Eur. Phys. J. C **1**, 509 (1998).

[5] A. Blondel *et al.*, Z. Phys. C **45**, 361 (1990).

[6] J. Allaby *et al.*, Z. Phys. C **36**, 611 (1985).

[7] E. A. Paschos and L. Wolfenstein, Phys. Rev. D **7**, 91 (1973).

[8] W. G. Seligman *et al.*, Phys. Rev. Lett. **79**, 1213 (1997).

[9] A. J. Buras and K. J. F. Gaemers, Nucl. Phys. B **132**, 249 (1978).

[10] M. Arneodo *et al.*, Nucl. Phys. B **487**, 3 (1997).

[11] E. A. Hawker *et al.*, Phys. Rev. Lett. 80, 3715 (1998).

[12] S. A. Rabinowitz *et al.*, Phys. Rev. Lett. 70, 134 (1993).

[13] D. Yu. Bardin and V. A. Dokuchaeva, JINR-E2-86-260 (1986); and private communication.

[14] CTEQ Collaboration, Phys. Rev. D **55**, 1280 (1997).

[15] L. W. Whitlow, SLAC-Report-357, 109 (1990).

[16] J. Pumplin, Phys. Rev. D **64**, 2751 (1990). $S_0 \leq 2$ GeV^2 is allowed by data summarized in M. Virchaux and A. Milsztajn, Phys. Lett. B **274**, 221 (1992).